

Identification and analysis of the Tl_2^+ ESR spectrum in $KCl:Tl^+$

Bai-rui Yang,* Etienne Goovaerts, and Dirk Schoemaker
Physics Department, University of Antwerp (UIA), B-2610 Wilrijk, Belgium
 (Received 3 August 1982)

The X-band electron-spin-resonance spectrum of the Tl_2^+ center, i.e., an electron trapped by a Tl^+-Tl^+ impurity dimer in heavily doped $KCl:Tl^+$, has been identified by the correlation of its formation and decay properties with those of the known Tl_2^+ optical-absorption bands. A spin-Hamiltonian fitting further supports this conclusion. A quantitative analysis of the hyperfine components shows that exchange polarization and s mixing both play an important role in the σ_g ground-state hyperfine interaction. A similar analysis of the g components yields the energies of the excited π_g states, and this combined with the optical-absorption data permits one to propose an energy-level scheme of the Tl_2^+ center in KCl .

I. INTRODUCTION

The electron- and hole-trapping properties of isolated Tl^+ , In^+ , and Ga^+ impurities in the alkali halides subjected to ionizing radiation have been extensively studied. The $Tl^+(6s^2)$ ion, in particular, has received a great deal of attention. Hole trapping results in $Tl^{2+}(6s^1)$ formation¹⁻³ while electron trapping at 77 K produces the primary $Tl^0(6s^26p^1)$ center,^{1,4} called $Tl^0(0)$.⁵ These Tl^{2+} and $Tl^0(0)$ defects both occupy unperturbed positive ion sites in the crystal. Recently complex Tl^0 , In^0 , and Ga^0 centers called $Tl^0(1)$, $Tl^0(2)$, etc., were investigated⁵⁻⁷; they involve one or more anion vacancies and they promise to be very interesting for the production of near-infrared color-center lasers.^{8,9}

In order to obtain high $Tl^0(1)$ center laser outputs the alkali halides are heavily doped with Tl^+ ions. However, with increasing Tl^+ impurity levels the concentration of nearest-neighbor Tl^+-Tl^+ pairs rises rapidly and these impurity dimers too can trap electrons and holes. The presence of these dimer centers introduces new optical-absorption bands which may interfere with the lasing properties of the crystals. It is therefore important to know the properties of these centers. The electron-spin-resonance (ESR) spectra of $\langle 110 \rangle$ -oriented Tl_2^{3+} species were observed recently in $KCl:Tl^+$ and they clearly represent holes trapped by Tl^+-Tl^+ dimers.¹⁰⁻¹² Some time ago the trapped electron dimer center Tl_2^+ was identified in $KCl:Tl^+$ by optical-absorption measurements.¹³ This work was confirmed and extended to other Tl^+ -doped alkali halides.¹⁴⁻¹⁶ In $KCl:Tl^+$ the Tl_2^+ center is characterized by optical-absorption bands at^{13,15} 460, 860, and 1760 nm.

This paper discusses the identification and analysis of the ESR spectra of the Tl_2^+ center in $KCl:Tl^+$. This is not a routine procedure because the Tl_2^+ hyperfine (hf) interaction is comparable to the X-band microwave energy that is being used and because isotope splittings are not resolved from the rather broad linewidth. Therefore, in Sec. III the production and decay of the ESR spectrum is shown to correlate with the behavior of the Tl_2^+ optical-absorption bands. In Sec. IV it is then proven that the ESR spectrum does indeed originate from a Tl_2^+ molecule ion. Finally, in Sec. V the Tl_2^+ electronic structure as derived from the ESR data is discussed and these results are combined with the optical data^{13,15} to propose an energy-level scheme for the Tl_2^+ center.

II. EXPERIMENTAL

The experimental procedures and the $KCl:Tl^+$ samples used were the same as in Ref. 5. We only recall here that several $KCl:Tl^+$ samples were used in the present investigation ranging in Tl^+ concentration from lightly doped ($\sim 1 \times 10^{-4}$ mol % of Tl^+) to heavily doped (2.2×10^{-2} mol % of Tl^+). The melts from which these crystals were grown contained at least an order of magnitude more Tl^+ .

III. CORRELATION OF THE Tl_2^+ OPTICAL-ABSORPTION AND ESR DATA

The ESR spectrum which we shall identify with the Tl_2^+ species in Sec. III is produced with easily observable intensities in $KCl:Tl^+$ crystals by a relatively short (~ 10 min) x irradiation at 77 K. It is important to notice that it is not or barely observed

in the lightly doped KCl crystals ($< 10^{-4}$ mol % of Tl^+), whereas it is very strongly produced in the heavily doped specimens ($\sim 2.2 \times 10^{-2}$ mol % of Tl^+). In optical-absorption measurements one notices the absence of, e.g., the 460-nm Tl_2^+ absorption band in the weakly doped crystals while this band is prominent in the heavily doped samples. Furthermore, in two specimens for which the Tl^+ concentration differed nominally by a factor of 5 the ESR intensity was about 30 times stronger in the more heavily doped specimens suggesting trapping by pairs of Tl^+ .

In order to establish more firmly the connection between the ESR spectrum and the 460-nm band pulse anneal experiments were performed with both techniques. Results obtained for the most heavily doped KCl: Tl^+ sample ($\sim 2.2 \times 10^{-2}$ mol % of Tl^+) are presented in Fig. 1. The Tl^0 center¹ [called the primary $Tl^0(0)$ center in Ref. 5] formed by simple electron trapping by a substitutional Tl^+ impurity, decays around 220 K by losing its electron. One notices in passing that this is about 40 K lower than in the lightly doped KCl: Tl^+ crystals.

As Tl^0 decays the 460- and 1760-nm Tl_2^+ bands increase substantially suggesting indeed the re-trapping of the freed electron by a Tl^+-Tl^+ dimer. Continuing, one observes the disappearance of the 460-nm Tl_2^+ absorption in the temperature region around 280 K. Figure 1 also presents the ESR data on a KCl: Tl^+ specimen cut from the same boule. It is seen that the change in ESR intensity parallels within experimental error the behavior of the 460-nm Tl_2^+ absorption band. The difference between the two types of data can be attributed to a slight difference in thermometry calibration between the two experimental setups. These experiments were repeated a few times, also in crystals with a somewhat lower Tl^+ concentration, and each time the correlation was confirmed. The only variation is that the decay temperatures were systematically shifted to somewhat higher values in the less strongly doped crystals.

The fact that the Tl_2^+ center concentration is high after a rather short x irradiation at 77 K underscores that it is produced by a simple electron trapping process and that no anion or cation vacancies are involved in the defect structure. Indeed, these vacancies become mobile only above 240 K (Refs. 5, 17, and 18) and the production of anion vacancies requires the creation of halogen interstitials, a process that is roughly an order of magnitude less efficient than electron-hole pair production.¹⁹

IV. ANALYSIS OF THE Tl_2^+ ESR SPECTRUM

The results of Sec. III as summarized in Fig. 1 strongly support the conclusion that the ESR spec-

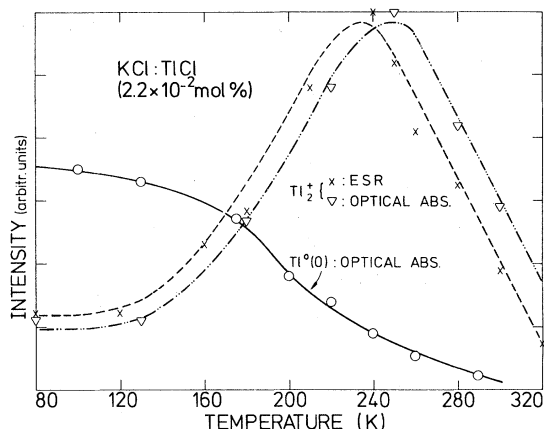


FIG. 1. Behavior of the Tl_2^+ ESR signal (\times), in a pulse anneal experiment showing that its creation [when the primary Tl^0 center (\circ) decays] and its decay coincide with the changes in the Tl_2^+ optical-absorption band (∇) at 460 and 1760 nm in a similar pulse anneal experiment. The KCl: Tl^+ crystals had, in both cases, first been x irradiated for 10 min at 77 K.

tra observed in strongly doped KCl: Tl^+ originate from a Tl_2^+ species. Therefore, these ESR spectra which are shown in Fig. 2 were fitted to a spin Hamiltonian of the form (usual notation)

$$\frac{\mathcal{H}}{g_0\mu_B} = \frac{1}{g_0} \vec{H} \cdot \vec{g} \cdot \vec{S} + \vec{S} \cdot \vec{A} \cdot (\vec{I}_1 + \vec{I}_2), \quad (1)$$

with $I_1 \equiv I_2 = \frac{1}{2}$, the value of the thallium nuclear spin. An angular variation of the spectra shows them to possess orthorhombic symmetry with a set of axes being, e.g., z || $[110]$, x || $[1\bar{1}0]$, and y || $[001]$. This is consistent with the D_{2h} symmetry of the Tl_2^+ center whose molecular axis z is along $\langle 110 \rangle$ (see Fig. 3). The ESR spectra in Fig. 2 are designated by the polar angles (θ, φ) of the external field with respect to a set of center axes (x, y, z) ; θ is measured from the internuclear axis z , and φ is measured from x .

Thallium has two isotopes both with nuclear spin $\frac{1}{2}$: ^{205}Tl which is 70 at. % abundant ($^{205}\mu_I = 1.6115$ nuclear magnetons) and ^{203}Tl which is 30 at. % abundant ($^{203}\mu_I = 1.5960$ nuclear magnetons). Ignoring isotope effects for a moment, the Tl_2^+ ESR spectrum should consist of three hyperfine lines with intensity ratios 1:2:1 provided the hyperfine term in (1) is much smaller than the Zeeman term. If \vec{A} is large the degenerate line will be split because of higher-order hf effects and a spectrum of four equally intense lines should be seen. A glance at Fig. 2 shows that the hf interaction is large and that the latter case should apply. Taking isotope effects into account one expects three Tl_2^+ species, i.e.,

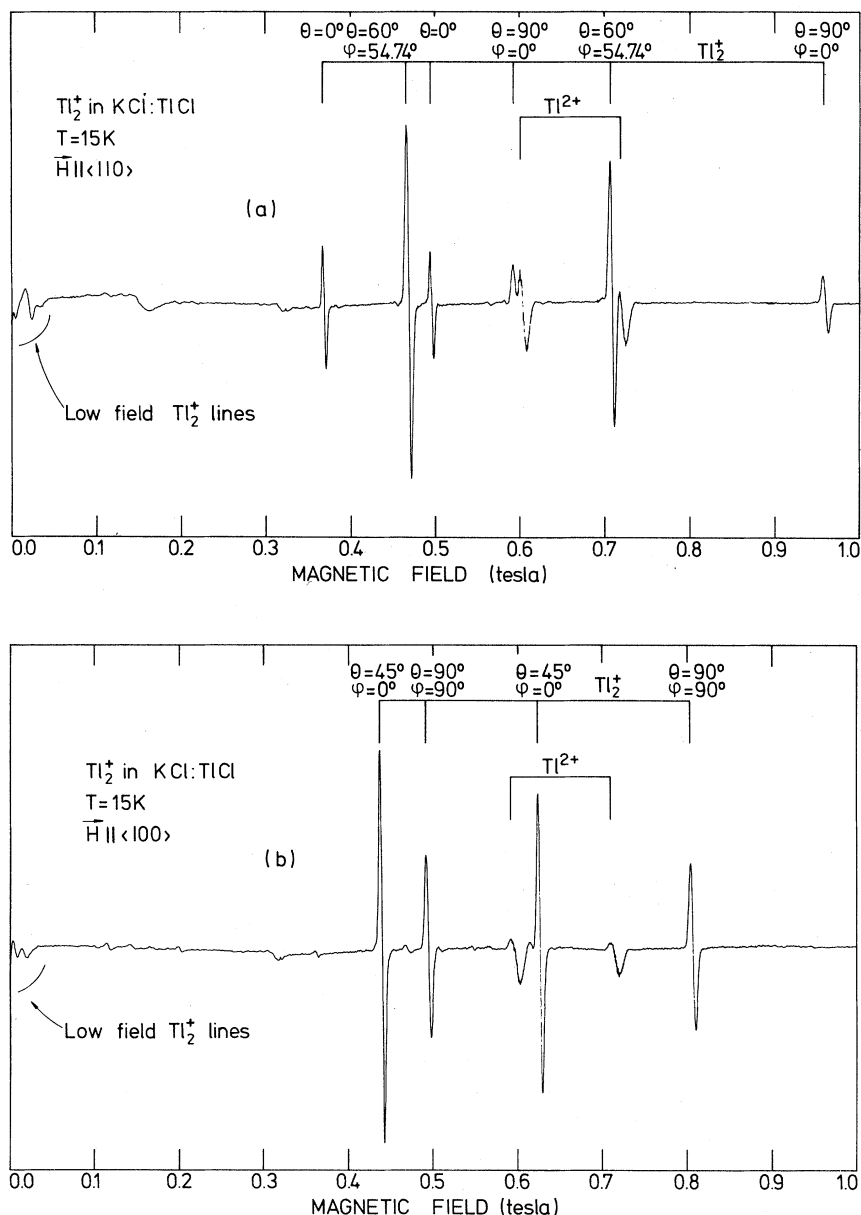


FIG. 2. Tl_2^+ ESR spectra in $KCl:Ti^+$ recorded at X -band frequency 9.16 GHz and at 15 K [(a) $\vec{H} \parallel \langle 110 \rangle$ and (b) $\vec{H} \parallel \langle 100 \rangle$]. Around this temperature the signal is most strongly observed. The sample had prior been x irradiated for 10 min at 77 K and warmed up to 240 K for about 2 min (see Fig. 1).

$(^{205}Tl-^{205}Tl)^+$, $(^{205}Tl-^{203}Tl)^+$, and $(^{203}Tl-^{203}Tl)^+$ with intensity ratios 49:42:9. No such isotope splittings are observed in the lines of Fig. 2, indicating that they must be smaller than the linewidth. The latter is considerable, varying between 4.0 and 6.0 mT. The quantitative fit of the spectra should confirm the absence of observable isotope splittings.

One obtains indeed a very good fit of the ESR spectra to spin Hamiltonian (1). The fitting procedure is not a trivial one because the hf interaction

with the two Tl nuclei is comparable to the X -band microwave energy. A numerical diagonalization of (1) is required together with a careful identification of the transitions involved.

The g and A components of $^{205}Tl_2^+$ as presented in Table I were obtained from a least-squares fitting of (1) to the ESR lines and the quality of the fit is illustrated in Table II.

It is seen that the fit is very good, differences between the observed and calculated line positions only

once amount to ~ 0.6 mT. Furthermore, the calculated isotope splitting between the almost equally abundant $(^{205}\text{Tl}-^{205}\text{Tl})^+$ and $(^{205}\text{Tl}-^{203}\text{Tl})^+$ never exceeds 20% of the experimental linewidth, making the splitting unobservable.

Figure 4 illustrates for $\theta=0^\circ$ ($\vec{H}||\langle 110 \rangle$) where the observed ESR transitions originate from. One rigorous selection rule independent of the relative strength of the hf interaction and the Zeeman energy is $\Delta I=0$ ($\vec{I}=\vec{I}_1+\vec{I}_2$) which is equivalent to a conservation of parity for the nuclear spin-wave functions.²⁰ For other differences it was verified by an explicit numerical calculation that their transition probabilities were negligible. Only the two solid double arrows in Fig. 4 correspond to strong transitions of comparable intensity. From this figure it is also seen that the hf interaction is comparable to the microwave energy. In fact, by sheer accident the zero-field hf splitting between the $F=\frac{3}{2}$, $m_F=\pm\frac{3}{2}$ and the $F=\frac{1}{2}$, $m_F=\pm\frac{1}{2}$ states ($\vec{F}=\vec{S}+\vec{I}$) is nearly identical to the 9.2-GHz microwave energy, and as Fig. 2 shows some very low-field (below 20 mT) ESR lines are observed. The broken double arrow in Fig. 4 indicates their origin. It was checked carefully that these low-field lines possessed exactly the same thermal formation and decay properties as the main Tl_2^+ ESR lines. Their presence thus underlines the correctness of the ESR analysis and its identification with Tl_2^+ .

It should be emphasized that the identification and analysis of this X-band ESR spectrum is not a trivial one. We have so far carefully avoided giving a qualitative analysis of the ESR patterns in Fig. 2, because in trying to do so one is inexorably led to an incorrect interpretation. Indeed, for every (θ, φ) spectrum in Fig. 2 one observes only *two* lines. Isotope splittings which might give a further clue are not resolved and consequently one is led to the conclusion that the ESR spectra originate from a species involving a single-Tl nucleus. In fact, one can analyze the spectra with a single-nucleus $I=\frac{1}{2}$ spin Hamiltonian and one obtains for the g components $g_z=1.4263$, $g_x=0.8056$, and $g_y=0.9633$. These numbers look reasonable and suggest that one would be dealing with a Tl^0 atom defect, because they resemble those of the $\text{Tl}^0(1)$ and $\text{Tl}^0(2)$ defects

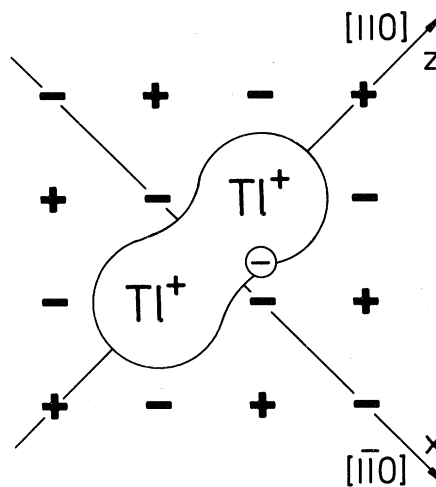


FIG. 3. Schematic two-dimensional model in a $\{100\}$ plane in KCl of the Tl_2^+ center, i.e., an electron trapped by a pair of substitutional Tl^+ ions. The $\langle 110 \rangle$ -oriented center possesses D_{2h} symmetry.

in KCl.⁵ The hf components in this analysis are $|A_z|=84.4$ mT, $|A_x|=147.1$ mT, and $|A_y|=144.3$ mT. These do not look so reasonable because they are roughly half the size of the $\text{Tl}^0(1)$ or $\text{Tl}^0(2)$ hf components.⁵

However, the additional reason for rejecting the single-nucleus $I=\frac{1}{2}$ spin-Hamiltonian description comes from a quantitative fit of the ESR lines exactly as for Tl_2^+ in Table II. When comparing these fits it is abundantly clear that the Tl_2^+ fit is superior. First, the calculated isotope splittings reach in this case 40% of the linewidth for some lines and this should be observable in the line shape. Second, the differences between the experimental and calculated line positions are consistently larger than in the Tl_2^+ case reaching ~ 1.7 mT in a few cases. Comparing the root-mean-square deviations one finds 0.28 mT for the Tl_2^+ fit, while it is 0.97 mT for the single $I=\frac{1}{2}$ nucleus fit, which is considerably worse. Finally, because of the much smaller calculated hf parameters in the Tl^0 type fit, no zero-field ESR lines should be observed while they are very clearly present in Fig. 2.

Thus, even on pure ESR grounds and not know-

TABLE I. Spin-Hamiltonian parameters of the $^{205}\text{Tl}_2^+$ center in KCl: Tl^+ at $T=15$ K. The hyperfine parameters and the linewidth ΔH (between points of maximum slope) are given in mT.

g_z [110]	g_x [1 $\bar{1}$ 0]	g_y [001]	A_z [110]	A_x [1 $\bar{1}$ 0]	A_y [001]	ΔH
1.7618	1.0997	1.3094	+ 190.4	-257.5	-259.3	5.0
± 0.0006	± 0.0005	± 0.0005	± 0.1	± 0.1	± 0.1	± 1.0

TABLE II. Comparison of the experimental and calculated ESR line positions of Tl_2^+ using the parameters of Table I and spin Hamiltonian (1). Also included are the experimental linewidth ΔH and the calculated isotope splitting (IS) between $(^{205}\text{Tl}-^{205}\text{Tl})^+$ and $(^{205}\text{Tl}-^{207}\text{Tl})^+$. All units are given in mT.

	$\theta=0^\circ$	$\theta=0^\circ$	$\theta=90^\circ$ $\varphi=0^\circ$	$\theta=90^\circ$ $\varphi=90^\circ$	$\theta=90^\circ$ $\varphi=90^\circ$	$\theta=45^\circ$ $\varphi=0^\circ$
H_{exp}	372.2	498.3	596.1	500.4	810.8	446.0
H_{calc}	371.9	498.2	595.8	500.4	810.8	446.1
ΔH	4.9	4.0		5.8	6.0	4.8
IS	0.01	0.29	0.02	0.02	1.2	0.01
	$\theta=45^\circ$ $\varphi=0^\circ$	$\theta=60^\circ$ $\varphi=54.74^\circ$	$\theta=60^\circ$ $\varphi=54.74^\circ$	$\theta=35.26^\circ$ $\varphi=90^\circ$	$\theta=35.26^\circ$ $\varphi=90^\circ$	$\theta=90^\circ$ $\varphi=35.26^\circ$
H_{exp}	631.4	471.1	709.6	403.2	564.0	557.5
H_{calc}	631.6	470.9	709.4	403.2	564.3	558.2
ΔH	5.3	5.0	6.0	5.0		
IS	0.53	0.01	0.81	0.01	0.44	0.02

ing the results of Fig. 1, one must conclude that a two-nuclei spin-Hamiltonian fit is superior to a one-nucleus fit and that the Tl_2^+ identification is correct.

V. ELECTRONIC STRUCTURE OF Tl_2^+

The discussion of the Tl_2^+ electronic structure will be based on a simple linear combination of atomic orbitals picture similar to the one used for the V_K center²¹ which is essentially a homonuclear X_2^- halogen molecule ion. In fact, the Tl_2^+ and X_2^- molecules possess for our purposes complementary electronic configurations: In X_2^- the eleven valence np ($n=2,3,4,5$) electrons of $X^0(np^5)$ and $X^-(np^6)$ are accommodated in six molecular orbitals according to the scheme $(\sigma_g)^2(\pi_u)^4(\pi_g)^4(\sigma_u)^1$.

In Tl_2^+ there is but a single- p valence electron ($\text{Tl}^0:6s^26p^1$ and $\text{Tl}^+:6s^2$) and only the bonding σ_g orbital is singly occupied. A very schematic orbital scheme of the Tl_2^+ is presented in Fig. 5.

The complementarity of the Tl_2^+ and X_2^- configurations means that the formal expressions for the g and hyperfine components as derived for X_2^- also apply to the Tl_2^+ case provided one changes the sign of spin-orbit coupling constant in these expressions. We refer to Ref. 21 for more details about the calculation.

A. g components

The Tl_2^+ g components can be written as (see Fig. 5)

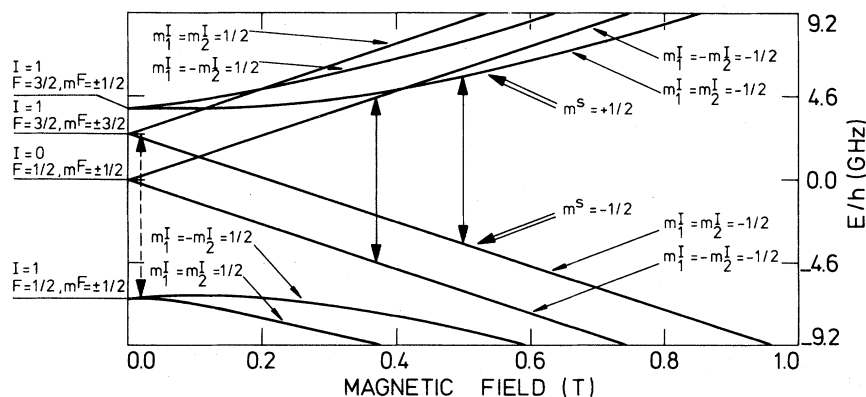


FIG. 4. Energy-level scheme of the Tl_2^+ ground state as a function of the magnetic field H for $\theta=0^\circ$, i.e., when the magnetic field is parallel to the Tl_2^+ molecular axis z . The solid vertical double arrowed lines identify the two main ESR transitions observable at X band and the broken double arrow indicates the very low-field ESR lines. Both types of Tl_2^+ lines are observed in Fig. 2.

$$\Delta g_z = g_z - g_0 = -\lambda_g^2 \left[\frac{1}{E_{1g}^2} + \frac{1}{E_{2g}^2} - \frac{\delta_z}{E_{1g}E_{2g}} \right], \quad (2a)$$

$$\Delta g_x = g_x - g_0 = -\frac{2a_g^2\delta\lambda_g}{E_{1g}} - \frac{2b_g^2\delta\lambda_g}{E_{2g}} - \lambda_g^2 \left[\frac{a_g^2}{E_{2g}^2} + \frac{b_g^2}{E_{1g}^2} \right] - \frac{\lambda_g\lambda'_g\delta}{E_{1g}E_{2g}}, \quad (2b)$$

$$\Delta g_y = g_y - g_0 = -\frac{2b_g^2\delta\lambda_g}{E_{1g}} - \frac{2a_g^2\delta\lambda_g}{E_{2g}} - \lambda_g^2 \left[\frac{b_g^2}{E_{2g}^2} + \frac{a_g^2}{E_{1g}^2} \right] - \frac{\lambda_g\lambda'_g\delta}{E_{1g}E_{2g}}, \quad (2c)$$

in which

$$\lambda_g = 2\mu_g\beta_g\lambda(TI^0), \quad (3a)$$

$$\lambda'_g = 2\mu_g^2\lambda(TI^0), \quad (3b)$$

$$a_g = k_g\lambda'_g,$$

$$b_g = k_g[\Delta_g + (\Delta_g^2 + \lambda_g'^2)^{1/2}],$$

where k_g is determined by $a_g^2 + b_g^2 = 1$, and Δ_g is the crystal-field contribution to the splitting of the π_g states. $\lambda(TI^0) = 5100 \text{ cm}^{-1}$ is the spin-orbit coupling constant of the $6p$ electron of the Tl^0 atom.⁵ The parameter δ is the value of orbital angular momentum between σ_g and π_g with a similar definition for δ_z between the π_g . For a free Tl_2^+ molecule δ_z is exactly 1, but if the excited π_g orbitals in the Tl_2^+ center would be somewhat delocalized over the surrounding ions, its value would be smaller. For δ one calculates

$$\delta = 2\beta_g\mu_g \left[1 - \frac{1}{2}(S_{\pi\pi} + S_{\sigma\sigma}) - \frac{1}{2} \frac{\alpha_g}{\beta_g} \left[R \left\langle 6s \left| \frac{\partial}{\partial x} \right| 6p_x \right\rangle - S_{\sigma s} \right] \right]$$

in which R is the Tl_2^+ internuclear distance, $\langle 6s | \partial/\partial x | 6p_x \rangle$ an atomic integral, and $S_{\pi\pi}$ and $S_{\sigma\sigma}$ and $S_{\sigma s}$ are overlap integrals. Inasmuch that the overlap integrals are $\ll 1$, δ is very well approximated by

$$\delta = 1 - \alpha_g\mu_g R \left\langle 6s \left| \frac{\partial}{\partial x} \right| 6p_x \right\rangle. \quad (4)$$

The value of δ depends very sensitively upon the molecular parameters, α_g in particular, which is very hard to calculate accurately (see Sec. VB). Es-

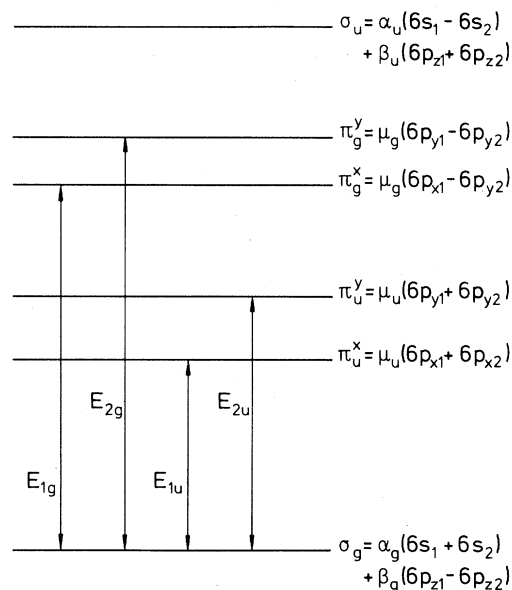


FIG. 5. Schematic valence orbital scheme of the free Tl_2^+ molecule ion with the single unpaired electron in the σ_g ground orbital.

timating $R(Tl_2^+)$ to be about 7 a.u. and using the X_2^- parameters as an approximation²¹ (in particular, $\alpha_g = 0.15$) one finds

$$\delta = 0.67. \quad (5)$$

This δ value is not unreasonable, but it is useless at this point to try to improve the accuracy of the estimation.

As in the case of the V_K center²¹ one can calculate an experimental δ value by combining the experimental g components of Table I with expressions (2). In an axial approximation

$$g_{\perp} = \frac{1}{2}(g_x + g_y) \quad \text{and} \quad (6)$$

$$E_{1g} = E_{1g} = E_{2g},$$

and assuming $\delta_z = 1$, one finds

$$\delta \approx 0.42, \quad (7)$$

which is surprisingly low. It should caution one not to try to push the accuracy of the analysis based on expressions (2).

Because the expression for Δg_{\parallel} is simpler, λ_g/E_{1g} will be calculated from it rather than from Δg_{\perp} . By doing so one avoids using the δ parameter which is not well known. However, the difficulty is now shifted towards the estimation of δ_z . Taking $\delta_z = 0.8$, i.e., assuming some delocalization for the excited π_g orbital, one finds

$$\frac{\lambda_g}{E_{1g}} = 0.45, \quad (8)$$

a value which is only 10% smaller than that when $\delta_z = 1$ would have been taken. Such changes are well within the expected precision of the present analysis and again it is useless to try to push it further. Note in passing that this λ_g/E_{1g} value increases the experimental δ value to about 0.50.

Taking the V_K center molecular coefficients again as an approximation one finds from (3a) that $\lambda_g \approx 4900 \text{ cm}^{-1}$ and thus from (8)

$$E_{1g} = 1.30, \quad (9)$$

expressed in units of eV. Furthermore, expressions (2b) and (2c) lead to

$$g_x - g_y = \frac{2\delta\lambda_g}{E_{1g}^2} \Delta_g,$$

from which $|\Delta_g| \approx 0.50 \text{ eV}$. This crystal-field splitting is comparable to the $\lambda_g = 0.61 \text{ eV}$ spin-orbit splitting and in lowest order the total separation of the two π_g states is given, again in eV, by²¹

$$E_{1g} - E_{2g} = (\lambda_g^2 + \Delta_g^2)^{1/2} = 0.79, \quad (10)$$

whence

$$E_{1g} \approx 1.70, \quad (11)$$

$$E_{2g} \approx 0.90. \quad (12)$$

B. Hyperfine components

The Tl_2^+ hf components including corrections up to second order are²¹

$$A_{||} = A_\sigma + 2\rho_s + 3 \frac{\lambda_g}{E_{1g}} \frac{\mu_g}{\beta_g} \rho_s - \frac{1}{2} \frac{\lambda_g^2}{E_{1g}^2} A_\sigma + 2 \frac{\lambda_g^2}{E_{1g}^2} \frac{\mu_g^2}{\beta_g^2} \rho_s + \frac{5}{2} \frac{\lambda_g^2}{E_{1g}^2} \frac{\mu_g^2}{\beta_g^2} \rho_l - \frac{\lambda_g^2}{E_{1g}^2} \rho_s, \quad (13a)$$

$$A_{\perp} = A_\sigma - \rho_s - \frac{3}{2} \frac{\lambda_g}{E_{1g}} \frac{\mu_g}{\beta_g} \rho_s - 5 \frac{\lambda_g}{E_{1g}} \frac{\mu_g}{\beta_g} \rho_l - \frac{1}{2} \frac{\lambda_g^2}{E_{1g}^2} A_\sigma + \frac{1}{2} \frac{\lambda_g^2}{E_{1g}^2} \rho_s - \frac{9}{4} \frac{\lambda_g^2}{E_{1g}^2} \frac{\mu_g^2}{\beta_g^2} \rho_s - \frac{5}{2} \frac{\lambda_g^2}{E_{1g}^2} \frac{\mu_g^2}{\beta_g^2} \rho_l, \quad (13b)$$

in which the anisotropic part ρ_s of the hf interaction is given by

$$\rho_s = \frac{2}{5} \frac{\mu_I}{I} \beta_g^2 \langle r^{-3} \rangle_s, \quad (14)$$

and $\rho_s \approx 1.13\rho_l$. The isotropic part A_σ will be dis-

cussed shortly. In (14) the value of $\langle r^{-3} \rangle_s$ is given by $1.07 \langle r^{-3} \rangle_{\text{hf}}$ where $\langle r^{-3} \rangle_{\text{hf}}$ is calculated over the $6p$ function of the Tl^0 atom. It can be calculated from expression (22) in Ref. 5 representing the Tl^0 hf components $A_{||}^{(1)}$ and $A_{\perp}^{(1)}$ calculated to lowest order. The hf components appropriate for a single- $6p$ Tl^0 function are obtained by applying the strong-crystal-field limit ($K_1 = 1/\sqrt{2}$ and $K_2 = -\sqrt{2}/\sqrt{3}$). Taking the traditional phase convention,^{6,7} which means changing the sign of $A_{\perp}^{(1)}$, one obtains the anisotropic part of the hf interaction from $A_{||}^{(1)} - A_{\perp}^{(1)}$. From this one finds $\langle r^{-3} \rangle_{\text{hf}} = 205 \times 10^{24} \text{ cm}^3$ and whence

$$\langle r^{-3} \rangle_s = 219 \times 10^{24}, \quad (15)$$

measured in cm^{-3} .

The ESR experiment does not yield the signs of the hf components. By inspecting the various sign combinations we have found that only the choice $A_{||} > 0$ and $A_{\perp} < 0$ as presented in Table I yields physically acceptable results. With this choice and using the results of Sec. VA one calculates from (13a) and (13b) that

$$A_\sigma = -14.5, \quad (16)$$

$$\rho_s = 44.7, \quad (17)$$

both in units of mT. It is hard to gauge the accuracy of these numbers, but $\pm 20\%$ would seem like an upper limit.

Combining (14), (15), and (17) one finds

$$\beta_g^2 \approx 0.32, \quad (18)$$

which is on the low side when compared to the corresponding quantity for the $X_2^- V_K$ center $\beta_g^2 = 0.41$. Still, the result is reasonable enough to permit the conclusion that the measured hf components of Table I are quite compatible with a Tl_2^+ species.

The low $\beta_g^2 \approx 0.32$ value may be caused at least partly by an accumulation of uncertainties in the parameters occurring in (13). It could, however, also reflect a delocalization of up to 30% of the unpaired σ_g orbital on the halogen ions surrounding the Tl_2^+ . This may seem quite large but then it should be stressed (see Table I) that the linewidth is very substantial, namely, $\sim 5.0 \text{ mT}$. This is too large to explain by simple dipole-dipole interaction between the σ_g unpaired electron spin and the surrounding halogen nuclear moments. Furthermore, Sn^+ , Ga^0 , In^0 , and Tl^0 centers in KCl exhibit covalency effects, with the np^1 electron residing up to 30% on one or more adjoining Cl^- ions.^{5-7,22} This makes a comparable delocalization of the Tl_2^+ σ_g electron quite plausible. If this is indeed so, then the excited orbi-

tals should be similarly delocalized. For π_g , in particular, this could result in a reduction of the δ_z value as discussed in Sec. V A. By the same token, the value of δ could be further reduced beyond the amount expressed by (5).

We now turn to the isotropic part A_σ of the hf interaction. If it is solely caused by s mixing into σ_g , A_σ is equal to

$$A_\sigma^s = \frac{8\pi}{3} \frac{\mu_I}{I} \alpha_g^2 |6s(0)|^2, \quad (19)$$

where $6s(0)$ is the value in the origin of the Tl atom $6s$ function. $A_\sigma \equiv A_\sigma^s$ should be positive, but as the experimental value (16) demonstrates this is definitely not the case for Tl_2^+ . Negative A_σ values are caused by exchange polarization effects and they can for Tl_2^+ formally be written as

$$A_\sigma^e = \frac{\mu_I}{I} \beta_g^2 \langle r^{-3} \rangle_c, \quad (20)$$

where $(\mu_I/I)\langle r^{-3} \rangle_c$ represents the exchange polarization contribution to the free Tl^0 atom hf interaction of the $6p$ valence electron. This value can be again obtained from formulas (22) in Ref. 5 by taking the strong-crystal-field limit ($K_1=1/\sqrt{3}$ and $K_2=-\sqrt{2}/\sqrt{3}$). Working with the traditional phase convention,^{6,7} which means changing the sign of $A_\perp^{(1)}$, one obtains from $\frac{1}{3}(A_\parallel^{(1)} + 2A_\perp^{(1)})$

$$(\mu_I/I)\langle r^{-3} \rangle_c = -110.7, \quad (21)$$

in units of mT, and according to (20) and using $\beta_g^2 \approx 0.32$ its contribution to the isotropic part of the Tl_2^+ hf interaction (again in mT) should be at least

$$A_\sigma^e = -35.4.$$

The difference between this value and experimentally determined one in (16) can be attributed to the mixing of $6s$ into $6p_z$ and so, in units of mT,

$$\frac{8\pi}{3} \frac{\mu_I}{I} \alpha_g^2 |6s(0)|^2 \cong 21.$$

This allows within the framework of this simple analysis a determination of α_g^2 provided $6s(0)$ of Tl^0 is known. We will not do this exercise because it is at best of limited quantitative value. We only emphasize that this analysis clearly shows that exchange polarization and s mixing both play an important part in the hf interaction in the σ_g ground state of Tl_2^+ .

C. Energy-level scheme of the Tl_2^+ center

The results of the g analysis as summarized in (11) and (12) can be combined with the optical-

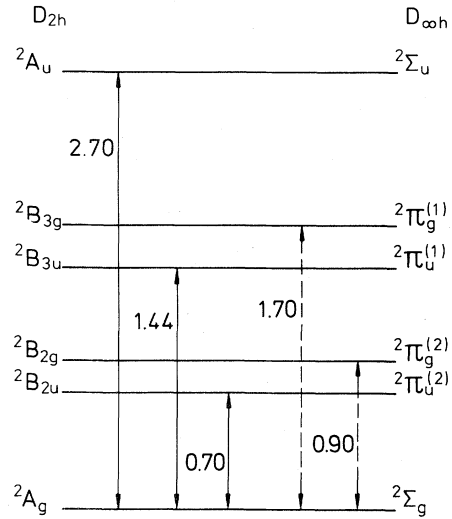


FIG. 6. Energy-level scheme of the Tl_2^+ center in $KCl:Tl^+$ as derived from the g -component analysis in this paper and the optical-absorption measurements (Refs. 13 and 15).

absorption data to propose an energy-level scheme for the Tl_2^+ center. In KCl , three Tl_2^+ optical-absorption bands have been identified^{13,15}: 460, 860, and 1760 nm, corresponding to the energies 2.70, 1.44, and 0.70 eV. It seems reasonable to identify the first transition with the $\sigma_g \rightarrow \sigma_u$ excitation and the remaining two with the $\sigma_g \rightarrow \pi_u$ transitions. The situation is summarized in Fig. 6. Note that if this identification is correct, the energy splitting of the π_u state is

$$E_{1u} - E_{2u} = 0.74 \text{ eV} = (\Delta_u^2 + \lambda_u'^2)^{1/2},$$

where $\lambda_u' = 2\beta_u \mu_u \lambda(Tl^0) \approx 0.67$ eV and so the crystal-field contribution Δ_u (in eV) to the splitting of π_u is

$$\Delta_u \cong 0.31.$$

The proposed level scheme in Fig. 6, though quite plausible, must of course be checked by more detailed investigations.

ACKNOWLEDGMENTS

The authors want to thank W. Van Puymbroeck for many discussions, A. Bouwen for excellent experimental support, and S. V. Nistor for growing some of the crystals. One of us (Y.B.-r.) is indebted to the Universitaire Instelling Antwerpen for a scholarship. Support from the Interuniversitair Instituut voor Kernwetenschappen, including a scholarship for E. G., is gratefully acknowledged.

*Permanent address: Department of Physics, Beijing University, Beijing, China.

- ¹C. J. Delbecq, A. K. Ghosh, and P. H. Yuster, *Phys. Rev.* **151**, 599 (1966); **154**, 797 (1967).
- ²W. Dreybrodt and D. Silber, *Phys. Status Solidi* **20**, 337 (1967).
- ³W. Frey, R. Huss, H. Seidel, and E. Werkmann, *Phys. Status Solidi B* **68**, 257 (1975).
- ⁴W. B. Hadley, S. Polick, R. G. Kaufman, and H. N. Hersh, *J. Chem. Phys.* **45**, 2040 (1966).
- ⁵E. Goovaerts, J. Andriessen, S. V. Nistor, and D. Schoemaker, *Phys. Rev. B* **24**, 29 (1981).
- ⁶W. Van Puymbroeck, J. Andriessen, and D. Schoemaker, *Phys. Rev. B* **24**, 2412 (1981).
- ⁷W. Van Puymbroeck, D. Schoemaker, and J. Andriessen, *Phys. Rev. B* **26**, 1139 (1982).
- ⁸W. Gellermann, F. Lüty, and C. R. Pollock, *Opt. Commun.* **39**, 391 (1981); W. Gellermann and F. Lüty, LASER 81 Conference, New Orleans, 1981 (unpublished).
- ⁹L. F. Mollenauer, N. D. Vieira, and L. Szeto, *Opt. Lett.* **9**, 414 (1982).
- ¹⁰T. Tsuboi, *Phys. Status Solidi B* **106**, 301 (1981).
- ¹¹Y. Toyotomi and R. Onaka, *J. Phys. Soc. Jpn.* **46**, 1861 (1979).
- ¹²Y. Toyotomi and R. Onaka, *J. Phys. Soc. Jpn.* **46**, 1869 (1979).
- ¹³C. J. Delbecq, E. Hutchinson, and P. H. Yuster, *J. Phys. Soc. Jpn.* **36**, 913 (1974).
- ¹⁴T. Tsuboi, *Can. J. Phys.* **54**, 2418 (1976).
- ¹⁵T. Tsuboi, *Can. J. Phys.* **57**, 1510 (1979).
- ¹⁶M. Roth and A. Halperin, *J. Phys. Chem. Solids* **43**, 609 (1982).
- ¹⁷F. Van Steen and D. Schoemaker, *Phys. Rev. B* **19**, 55 (1979).
- ¹⁸E. Goovaerts, S. Nistor, and D. Schoemaker, *Phys. Rev. B* **25**, 83 (1982).
- ¹⁹See, e.g., W. Van Puymbroeck and D. Schoemaker, *Phys. Rev. B* **23**, 1670 (1981).
- ²⁰D. Schoemaker, *Phys. Rev.* **174**, 1060 (1968).
- ²¹D. Schoemaker, *Phys. Rev. B* **7**, 786 (1973).
- ²²C. J. Delbecq, R. Hartford, D. Schoemaker, and P. H. Yuster, *Phys. Rev. B* **13**, 3631 (1976).